Excited State Intramolecular Proton Transfer Dynamics for Triplet Harvesting in Organic Molecules

Y. Cao, J. Eng, and T.J. Penfold*

Chemistry- School of Natural and Environmental Sciences, Newcastle University, Newcastle upon Tyne, NE1 7RU, UK.

E-mail: tom.penfold@ncl.ac.uk

Abstract

Thermally activated delayed fluorescence (TADF) has shown great potential as a mechanism for harvesting low-lying triplet excited states in organic molecules and is therefore of great interest in the context of organic electronics, especially organic light emitting diodes (OLEDs). Herein we study the mechanism for triplet harvesting in triquinolonobenzene (TQB), which instead of relying upon the well-established donor-acceptor (D-A) scheme uses excited-state intramolecular proton transfer (ESIPT). We demonstrate that upon photoexcitation into the lowest singlet excited state the proton is transferred within 20 fs, suggesting it plays little role in triplet harvesting which occurs on the nano- to micro-second timescale. However, TQB exhibits multiple low-lying triplet states that are strongly coupled along this proton transfer coordinate. The majority of these states favour the structure prior to proton transfer (TQB-TA) and this means that the proton transfer dynamics (^{3}TQB-TA$\rightarrow$^{1}TQB-TB) plays a crucial role in triplet harvesting. This mechanism yields an energy gap in good agreement with

that reported experimentally and is consistent with previous photophysical characterisation. Finally, a discussion upon extending this understanding into a device context is also presented.

1 Introduction

Thermally activated harvesting of low-lying non-emissive triplet excited states is an active area of research with many potential applications across organic electronics, including light emitting diodes,[1,2] lasers[3,4] and photovoltaics.[5,6] This interest is driven by the fact that for organic systems, the weak coupling between triplet and singlet states means that triplet states can often act as low energy trapping sites, ultimately leading to unwanted processes which are detrimental to device performance.

To date, the most successful design strategies for organic triplet harvesters have focused upon intra-/intermolecular donor-acceptor (D-A) systems exhibiting charge-transfer (CT) transitions.[7] This minimises the exchange energy between singlet and triplet states of the same character providing a small enough energy gap to permit thermal activation of harvesting.[8] In the context of organic light emitting diodes (OLEDs), while these D-A molecules are able to achieve 100% internal quantum efficiency,[9] the use of CT states means that the radiative rate is usually low[10] leading to long excited state lifetimes and consequently instability and reduced device performance associated with excited state quenching mechanisms.[11] In addition, the electroluminescence (EL) from these molecules is inherently broad, with a typical full-width at half-maximum (FWHM) $\sim$70-120 nm. This width reduces colour purity, making them difficult to use in displays, which require a FWHM $<$30 nm.

To overcome this, Hatakeyama *et al.*[12] have developed an approach that reduces the energy gap between the singlet and triplet states by exploiting the opposite resonance effect of nitrogen and boron atoms in a para-substitution arrangement. This can separate the highest occupied molecular orbital (HOMO) and lowest unoccupied molecular orbital (LUMO) without the need to introduce donor or acceptor groups, making it possible to design rigid

molecules that exhibit a very narrow FWHM. However, the rigidity of the molecule restricts the triplet harvesting[13] limiting device performance, especially at normal brightness levels where a large roll-off in the efficiency is observed.[12] This is expected within the framework of the spin-vibronic mechanism[14] for efficient triplet harvesting, which shows that the small mixing between singlet and triplet states due to spin-orbit coupling can be enhanced by the coupling to multiple excited states driven by specific molecular vibrations.[15–17] Importantly in the case of rigid molecules these vibrations are obviously reduced, quenching the triplet harvesting rate.

To diversify molecular design approaches for thermally activated delayed fluorescence (TADF) materials which are required to overcome some of the aforementioned limitations, Mamada *et al.*[18] have investigated the possibility for triplet harvesting by excited state intramolecular proton transfer (ESIPT). In this process, photoexcitation drives the transfer of a hydrogen atom covalently bonded to one heteroatom to a second on the same molecule. This causes a separation of the HOMO and LUMO reducing the energy gap between the low lying excited states. The effect of ESIPT is well documented[19] and solvatochromism, indicative of a state of CT characteristics, in the emission of such materials has been widely reported.[20,21] Indeed, TADF from ESIPT materials in solution have previously been reported by Park *et al.*[22] This arises from a small energy gap of 0.06 eV between the singlet and triplet state and leads to a rate of reverse intersystem crossing (k_{rISC}) of $\sim 10^7$ s^{-1}. However, in this case the large amplitude structural rearrangements of the molecule were required to enable ESIPT and therefore TADF. While this does not affect the solution phase measurements of Park et al.,[22] it represents a severe limitation for triplet harvesting in OLEDs, which exist in the solid state[23] and would therefore constrain the larger amplitude motions required. Importantly, the molecule, triquinolonobenzene (TQB, Figure 1) developed by Mamada *et al.*[18] demonstrated ESIPT for a rigid structure, and was able to harvest a large contribution of the triplets states, achieving up to $\sim$14% external quantum efficiency (EQE) when integrated into an OLEDs.

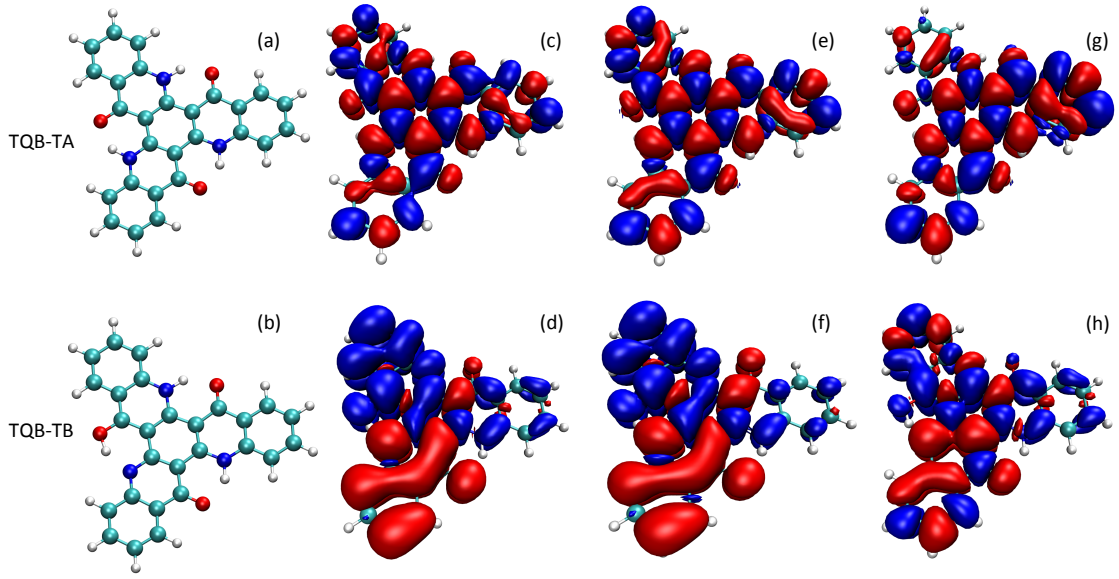

Figure 1: The structure of TQB-TA (a) and TQB-TB (b). The density differences ($\Delta\rho = \rho_{S_1} - \rho_{S_0}$) for the S_1 state at the TQB-TA (c) and TQB-TB (d) geometries, the T_1 state at the TQB-TA (e) and TQB-TB (f) geometries and the T_2 state at the TQB-TA (e) and TQB-TB (f) geometries. Colour Code: Cyan= Carbon, Red=Oxygen, Blue= Nitrogen and White=Hydrogen.

This high EQE is encouraging for a new emitter design, especially given the slow reverse intersystem crossing rate (k_{rISC}) of $\sim 10^3$ s^{-1}. Consequently, a detailed understanding of the triplet harvesting mechanism could provide the basis to significantly enhance the performance of ESIPT TADF emitters. In this paper we combine quantum chemistry, molecular and quantum dynamics to study the excited state processes and triplet harvesting mechanism in TQB. We show that despite the proton transfer in the singlet excited state occurring on a timescale much faster than intersystem crossing (ISC), it plays a crucial role in the triplet harvesting. This arises due to multiple low-lying triplet states that are strongly coupled along the proton transfer coordinate and tend to favour the structure without proton transfer (TQB-TA). A model Hamiltonian is developed and used to simulate the absorption spectrum and corresponding excited state dynamics. We find an intersystem crossing rate which is in good agreement with that reported experimentally and shows a splitting of the wavepacket in the triplet state between the TQB-TA and proton transferred TQB-TB forms. Finally, a discussion upon the dynamics involved in electroluminescence important for a device is also

presented.

2 Methods

2.1 Quantum Chemistry

The geometry of TQB in its ground and relevant excited states were calculated using density functional theory (DFT) and linear response time-dependent density functional theory (LR-TDDFT) within the Tamm-Dancoff approximation[24] and the PBE0 exchange and correlation functional[25,26] as implemented within the Q-Chem quantum chemistry package.[27] A Def2-SVP[28] basis set was used throughout and the solvent was described using conductor-like polarisable continuum model[29] with the dielectric constant of toluene. Emission energies, calculated using the S_1 optimised geometries included a state-specific polarisable continuum model (SS-PCM).[30] For the SS-PCM, the energy of both the S_1 and ground state were calculated within an S_1 optimised solvation structure, yielding the vertical emission energy.

2.2 *Ab initio* Molecular Dynamics

Ab initio molecular dynamics (AIMD) of TQB in its electronic ground and excited singlet (S_1) state were performed using the Terachem package.[31,32] The potential energy and forces was calculated using DFT(PBE0) and a 3-21G* basis set. The effect of the environment was included using a conductor-like polarisable continuum model[29] with the dielectric constant of toluene. The MD was performed using a microcanonical (NVE) ensemble using initial velocities sampled at random from a Boltzmann distribution of velocities at 300K. 20 configurations selected at random from 10 ps of ground state MD were used as starting points to compute the excited state dynamics in the S_1 state. Each of these was run for 5 ps. 40 different configurations from the ground state MD were used to simulate the absorption spectrum, while excited state geometries were used to simulate the emission spectrum. The total absorption and emission spectra was generated by summing the contributions of each

spectrum for which the oscillator strength had been broadened by a Gaussian function with a 0.02 eV or 0.05 eV full width half maximum for the absorption and emission spectra, respectively.

2.3 Quantum Dynamics

The nonadiabatic excited state quantum dynamics of TQB were investigated using a model Hamiltonian operator based upon the Spin-Vibronic Coupling Hamiltonian[14] ($\mathbf{H}^{SO-vib}$). This Hamiltonian is the sum of a non-relativistic vibronic coupling Hamiltonian matrix ($\mathbf{H}^{vib}$), and spin-orbit, ($\mathbf{H}^{SO}$) Hamiltonian matrices:

$$\mathbf{H}^{SO-vib} = \mathbf{H}^{vib} + \mathbf{H}^{SO} \tag{1}$$

$\mathbf{H}^{SO}$ is comprised of off-diagonal spin-orbit coupling terms, which can either be Q-dependent[33] or independent.[34] Where Q represents the dimensionless (mass-frequency scaled) normal mode coordinates. In this present work, the spin-orbit coupling terms are Q-dependent along the proton transfer mode as described in the supporting information.

The vibronic coupling Hamiltonian matrix is expressed:

$$\mathbf{H}^{vib} = (T_N + V_0)\mathbf{1} + \mathbf{W} \tag{2}$$

T_N is the kinetic energy operator. In the absence of large-amplitude motions as in the case here for a rigid molecule, a model potential in terms of a subset of the ground state normal modes can be determined. In the present case, the normal modes are evaluated at the mid-point of the proton transfer geometry. This choice of coordinates simplifies the construction of the Hamiltonian as the kinetic energy operator has a simple separable form.[35]

V_0 is the ground state potential and defined as a harmonic oscillator with vibrational frequencies ω_i corresponding to dimensionless normal coordinate Q_i. $\mathbf{W}$ is the diabatic coupling matrix which is expanded as a Taylor series up to 4^{th} order in the present work.[36,37]

This matrix contains both on and off-diagonal elements. The on-diagonal elements are the forces acting within an electronic surface and are responsible for structural changes of excited-state potentials compared to the ground state. The off-diagonal elements are the nonadiabatic couplings responsible for transferring wavepacket population between different excited states. The parameters for these matrices are obtained from a fit to quantum chemistry points calculated along and diagonally between the normal modes displacements. The parameters obtained from this fit and a description of the model Hamiltonian can be found in the supporting information. All dynamics were performed using the multi-configuration time-dependent Hartree (MCTDH) method as implemented in the Quantics quantum dynamics package.[38,39] The details of the calculation are given in Table S4. The calculations are initiated in the S_1 state by projecting the wavefunction, built using one-dimensional harmonic oscillator functions with zero initial momentum, into the lowest energy geometry of the S_1 state, the TQB-TB form.

The absorption spectrum of TQB was simulated using the Fourier transform of the autocorrelation function written:

$$I(\omega) \sim \int_{-\infty}^{\infty} C(t) \exp^{-i\omega t} \, dt, \tag{3}$$

where $C(t)$ is the autocorrelation function. Before the autocorrelation function is transformed it is modified slightly. To reduce artefacts associated with the finite propagation time (temporal truncation) which causes ringing artefacts in the spectrum, due to taking the Fourier transform only over a finite time interval (Gibbs phenomenon), the autocorrelation function is multiplied by $\cos^2(n\pi t/2T)$, where $n = 1, 2, \ldots$ and T denotes the final time plus one time step of the autocorrelation function. The autocorrelation function is calculated as:

$$C(t) = \langle \psi_i(0) | \psi_f(t) \rangle, \tag{4}$$

where $\psi_i(0)$ is the initial wavefunction in the ground state and $\psi_f(t)$ is the time-dependent

wavefunction in the excited state. The total spectrum is a sum of spectra generated in this way with weighting of $\exp(-t/\tau)$, where τ is the damping function applied to the autocorrelation function, in this case 20 fs.

3 Results

In the following sections we present a characterisation of the ground and excited state structures of TQB (Figure 1), followed by its excited state properties. Subsequently, using molecular and quantum dynamics we study its photophysics. Finally, we present a perspective of how the excited state behaviour alters in the case of electrical excitation compared to optical excitation and propose how this influences the triplet harvesting properties in OLEDs.

3.1 Ground and Excited State Structures

TQB can exist in two major tautomers, TQB-TA (Figure 1a) and TQB-TB (Figure 1b). Although Mamada *et al.*[18] also reported structures involving multiple sequential proton transfers, these are much higher in energy and are therefore considered unlikely. Table 2 shows the optimised structures of each form. As expected, the structure is planar in all cases. In the electronic ground state (S_0) the main structural parameters around the proton transfer site are in good agreement with the X-ray diffraction reported in ref.[18] The one exception is the hydrogen bond parameters. However, the assignment of the position of this proton is complicated by crystal disorder. The geometry of TQB in the present work is in good agreement with calculations presented in ref.[18]

Upon excitation into the S_1 state, a stable form of TQB-TA can be optimised and exhibits similar properties to the ground state. However, the lowest energy geometry of the S_1 state is the TQB-TB tautomer, with the proton transferred from the nitrogen to the oxygen. This structure indicates a compression of the O-H distance by 0.68 Å, elongation of the C-O bond and a slight change in the C-N-H and C-O-H bond angles involved in the proton transfer.

The lowest triplet excited state (T_1), like the singlet state, exhibits stable minima in the TQB-TA and TQB-TB tautomers, but again the lowest energy conformer is TQB-TB. In this case the change in energy is not so large owing to a change in character of this state along the proton transfer coordinate, as discussed below.

Table 1: Main structural parameters of optimised geometries of stable TQB-TA and TQB-TB tautomers in the ground (S_0) and excited singlet (S_1) and triplet (T_1) states. The molecular structure TQB-TB is not stable in the ground state and thus we could not find the stationary point of its S_0 form. The structure of TQB-TA from ref.[18] corresponds to the one obtained using X-ray Diffraction of the crystal structure.

		S_0	T_1		S_1	
	TQB-TA[18]	TQB-TA	TQB-TA	TQB-TB	TQB-TA	TQB-TB
N-H (Å)	0.88	1.04	1.04	1.66	1.04	1.66
O-H (Å)	1.91	1.68	1.68	1.00	1.69	1.00
C-O (Å)	1.25	1.24	1.25	1.33	1.25	1.33
C-C (Å)	1.44	1.44	1.43	1.42	1.42	1.44
C-N-H (°)	116.0	113.5	112.8	102.2	112.9	103.0
C-O-H (°)	102.3	103.0	103.4	106.2	103.6	105.9

Table 2 demonstrates that despite the large Stokes shift in the emission,[18] initiated by the ESIPT process, the structural changes of the TQB in the excited state are small and almost completely localised to the hydrogen bond lengths and angles. This is important in the context of developing a reduced coordinated model Hamiltonian as shown below.

3.2 Excited State Properties

Table 3 shows the excited state energies of the important low lying states of TQB-TA and TQB-TB at the ground (S_0), excited singlet (S_1) and triplet (T_1) state geometries identified in Table 2. At the TQB-TA ground state geometry, the lowest singlet states is at 3.57 eV, and as shown in Figure 1b corresponds to an excitation that is delocalised over the whole molecule. However, despite the apparent overlap between the HOMO and LUMO seen in the density difference plot, the oscillator strength (f_{S_1}) for this transition is zero.

The zero oscillator strength of the S_1 state at the Franck-Condon geometry means that the lowest band in the absorption spectrum must gain intensity through vibronic mixing.

Table 2: Calculated vertical excitation energies, oscillator strengths and energy gaps at the stable TQB-TA and TQB-TB tautomers in the ground (S_0) and excited singlet (S_1) and triplet (T_1) states.

	S_0	T_1		S_1	
	TQB-TA	TQB-TA	TQB-TB	TQB-TA	TQB-TB
E_{T_1} (eV)	3.03	2.93	2.14	2.94	2.25
E_{T_2} (eV)	3.16	3.07	2.66	3.08	2.67
E_{T_3} (eV)	3.16	3.07	2.77	3.09	2.81
E_{T_4} (eV)	3.28	3.20	2.95	3.18	2.95
E_{S_1} (eV)	3.57	3.48	2.57	3.47	2.59
E_{S_2} (eV)	3.75	3.67	3.23	3.65	3.28
f_{S_1}	0.00	0.00	0.25	0.00	0.20
$\Delta E_{S_1-T_1}$	0.54	0.55	0.43	0.53	0.34
$\Delta E_{S_1-T_2}$	0.41	0.41	-0.08	0.39	-0.08

Figure 2 shows the absorption and emission spectra calculated from sampling ground and excited state configurations using AIMD. The calculated absorption spectrum, shifted down in energy by 0.1 eV, shows good agreement with the experimental spectrum. The vibronic transitions observed are in agreement with the experimental spectrum. These are separated by 0.14 eV, corresponding to a timescale of $\sim$ 30 fs and originate from the motion associated with the proton transfer. Indeed, while the oscillator strength of the S_1 state is zero at the TQB-TA geometry, as shown in Table 2, proton transfer, forming TQB-TB significantly increases this oscillator strength and therefore this motion is responsible for making this transition allowed. It is interesting to note that this is unique amongst normal TADF materials, as in many cases, the excited state motion making the S_1 state more CT reduces the energy gap between the singlet and triplet states and makes the radiative rate smaller.

The emission spectrum is also in very good agreement with the experimental spectrum recorded in toluene.[18] Despite the rigidity of the molecule, the emission spectrum is rather broad with the calculated FWHM of 0.35 eV close to the experimentally observed value of 0.40 eV. This width derives from the large effect the motion of the proton has on modulating the gap between the ground and excited states. This calculated emission spectrum includes a SS-PCM model. Here, both the S_1 and ground state were calculated within an S_1 optimised

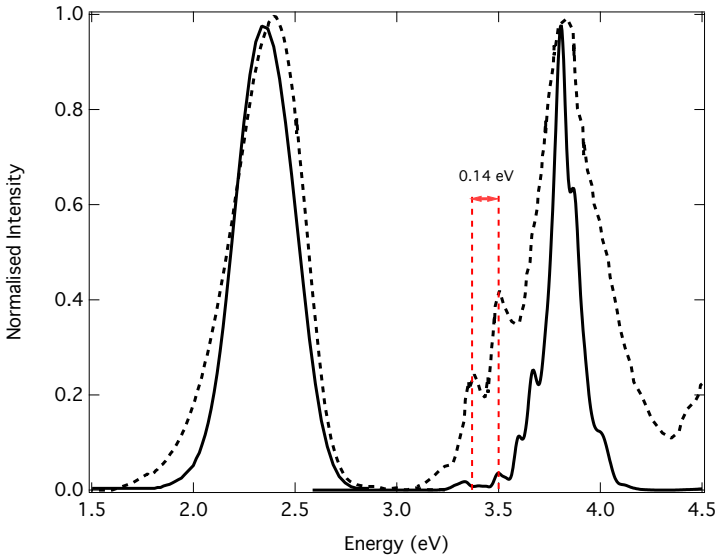

Figure 2: The experimental absorption and emission spectra (dashed)[18] compared to those calculated (solid) by sampling configurations using molecular dynamics simulations as described in the methods section. The absorption spectrum has been shifted down by 0.1 eV to overlap the main absorption peaks and facilitate the comparison between the experimental and calculated spectra.

solvation structure, yielding the vertical emission energy including the effect of slow solvation dynamics adjusting to the new dipole (∼5 D) of the S_1 state. When the dielectric constant is changed to THF and DMF, a stabilisation of the S_1 excited state by 0.06 and 0.12 eV, respectively, is observed, matching that observed experimentally[18] and reflecting that the effect of polarity is weaker than for many TADF emitters due to the smaller excited state dipole moment. Importantly, in the solid state, no shift in the emission is observed even for high polar hosts such as DPEPO. This is consistent with the amorphous guest-host film expected and the concepts of solid state solvation.[40]

Finally Table 3 shows the spin-orbit coupling matrix elements (SOCME) between the lowest singlet and triplet states. This is crucial for the coupling between the singlet and triplet manifolds and therefore triplet harvesting. At the TQB-TA structure, the SOCME are all very small and can be considered negligible, with the exception of S_1-T_1 = 1.2 cm^{-1}. However, upon proton transfer there is a notable increase for the coupling between all states except S_1-T_1 which decreases to 0.2 cm^{-1}. This is because the S_1 and T_1 state at the TQB-TB

Table 3: Calculated spin-orbit coupling matrix elements (SOCME) in cm^{-1} between the lowest singlet and triplet states. These were calculated using TDDFT(PBE0) at the optimised ground state geometry of TQB-TA and optimised S_1 state geometry of TQB-TB.

		T_2	T_3	T_4	S_1
TQB-TA(S_0)	T_1	0.002	0.004	1.017	1.198
	T_2	-	1.021	0.005	0.003
	T_3	-	-	0.004	0.006
	T_4	-	-	-	0.362
	S_1	-	-	-	-
TQB-TB(S_1)	T_1	0.884	0.907	0.385	0.231
	T_2	-	0.343	0.513	0.796
	T_3	-	-	0.111	0.131
	T_4	-	-	-	0.023
	S_1	-	-	-	-

geometry are very similar characters and therefore the change in spin cannot be compensated by a change in orbital angular momentum, meaning SOCME is close to zero. Importantly, these small couplings are the main source for the slow ISC rate and correspondingly slow triplet harvesting.

3.3 Excited State Dynamics

In ESIPT, a hydrogen atom is covalently bonded to one heteroatom and hydrogen bonded to a second in the same molecule. Photoexcitation drives the proton transfer so that the hydrogen becomes bonded to the second heteroatom and hydrogen bonded to the first. Figure 3 shows the average and standard deviation of the O-H bond distance obtained from excited state MD in the S_1 state performed using 20 different initial conditions.

This shows ultrafast proton transfer consistent with the relaxed excited state potential surface calculated along the proton transfer coordinate and shown in Figure 4. The barrier observed in the S_1 state is $\sim$0.03 eV, comparable to thermal energy at 300 K. The proton transfers within $\sim$ 20 fs (Figure 3), approximately one vibrational period of the proton transfer. Small oscillations, with a similar period, corresponding to the vibronic fine structure observed in the absorption spectrum, are subsequently observed. However, after the initial

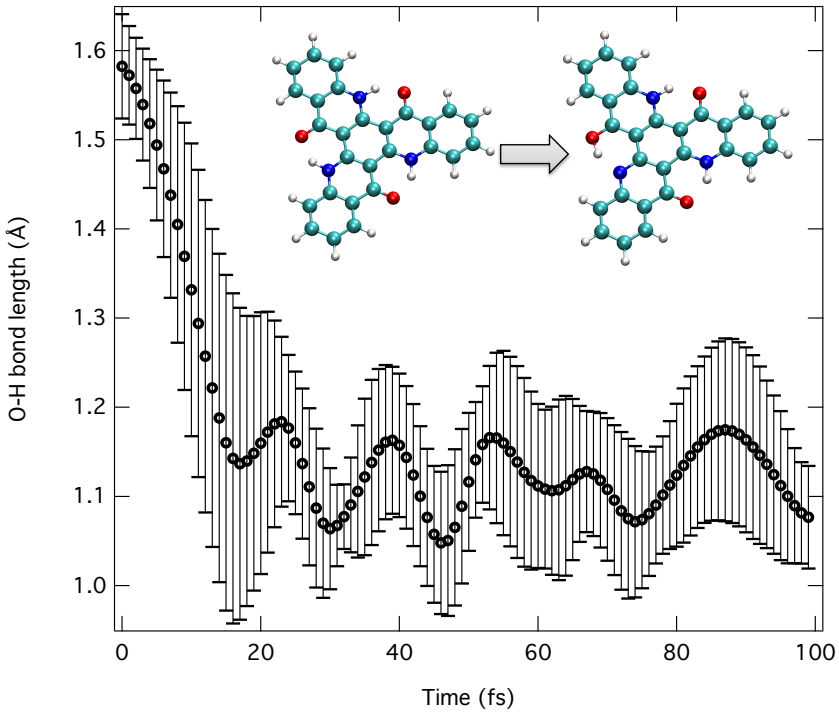

Figure 3: The average and standard deviation (error bars) of the O-H bond distance for the transferred proton obtained from 100 fs of excited state molecular dynamics in the S_1 state for 20 different starting configurations. Insets show snapshots of the structure before and after proton transfer.

20 fs, the hydrogen remains localised in the TQB-TB form.

It is important to notice that although the relaxed excited state potential surface for the S_1 state is almost barrier-less, a barrier of almost 0.2 eV is observed in the lowest triplet state (Figure 4). This is confirmed using excited state MD in the T_1 state, during which no proton transfer is observed from the TQB-TA to TQB-TB form. This barrier is responsible for trapping some triplet population in the TQB-TA form, which becomes very relevant in the context of triplet harvesting discussed later.

The dynamics shown in Figure 3 only consider the singlet state and not the role of the triplets. As shown in previous works[15–17] multiple triplet states and the coupling between them can be important for enhancing the singlet-triplet mixing and therefore in the context of triplet harvesting. To understand the present system, we develop a model spin-vibronic Hamiltonian to describe the dynamics in TQB. Figure 5 shows the 2 normal modes used

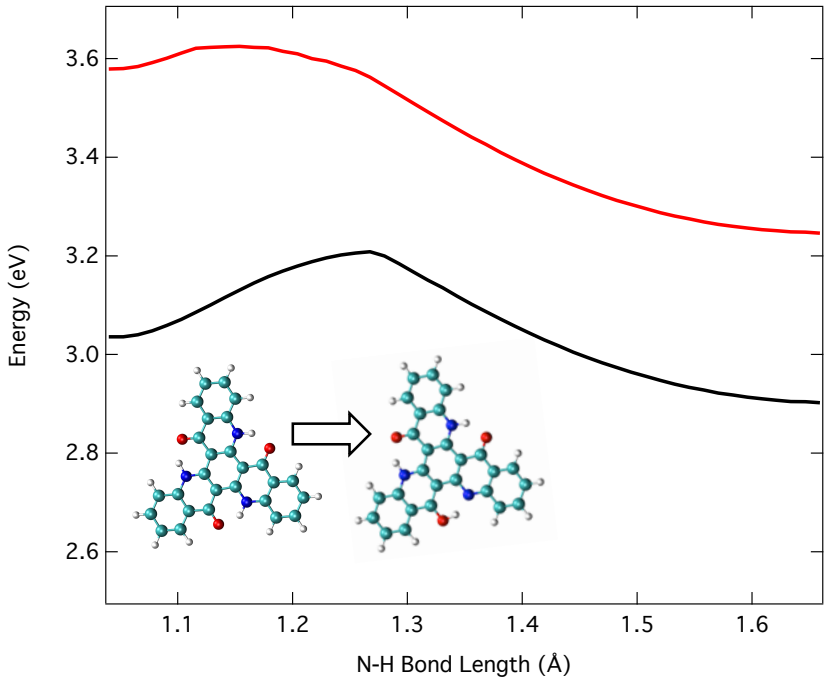

Figure 4: Relaxed excited state potential pathway along the S_1 (red) and T_1 (black) states calculated at TDDFT(PBE0) level of theory.

for the Hamiltonian. These were selected on the basis that they capture the geometric changes in the excited state shown in Table 2. The first, ν_1 corresponds to the motion of the proton between the oxygen and nitrogen atoms. The second normal mode, ν_{124} shows the angle change between the proton and the bonding atoms. Their respective ground and excited state potential energy surfaces are shown in Figure 6. The points are the quantum chemistry calculations and the lines are the fit of a 4^{th}-order vibronic coupling Hamiltonian to these points. It is from these fits that the parameters (shown in the supporting information) for the Hamiltonian used in the quantum dynamics are obtained.

For the potential along ν_1 (Figure 6) the S_1 state (red) shows a smooth transition from the TQB-TA to the TQB-TB conformer, as expected from the AIMD simulations. In contrast the triplet states show a rather more complicated profile with multiple curve crossings between the lowest four triplet states. Indeed, this clearly shows a crossing between the T_1 and T_2 states which is responsible for the barrier observed in Figure 4. Along ν_{124}, the potentials are much simpler, with the excited state potentials slightly shifted with respect to the ground

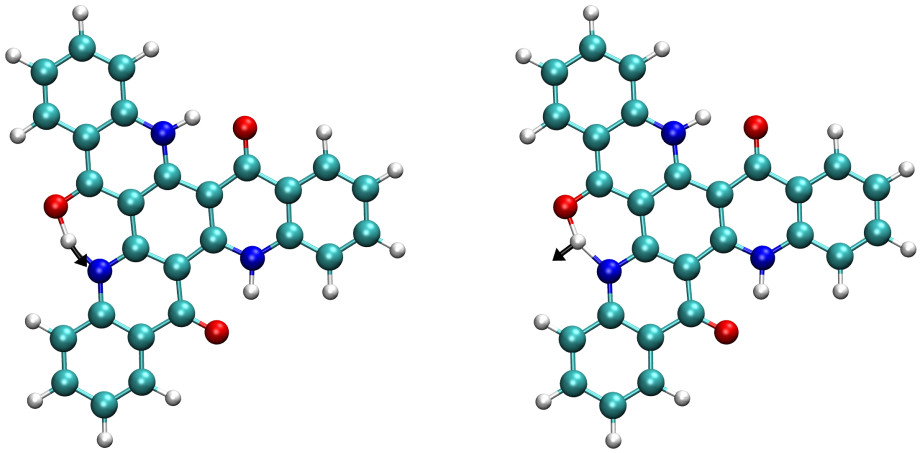

Figure 5: The 2 normal modes, ν_1 (left) and ν_{124} (right) used for the model spin-vibronic Hamiltonian. The arrow represents the atomic motion associated with the normal mode.

state. Consequently, upon excitation, this mode will drive a structural change leading to a decrease in the C-N-H consistent with the structural parameters reported in Table 1. The parallel nature of the potential energy curves along this mode indicates that there is little or no non-adiabatic coupling. This mode can therefore be considered a tuning mode, in the sense that it purely changes the energy gap between the ground and excited states. ν_1 on the other hand exhibits large coupling, and is responsible for the mixing between the low lying triplet excited states.

To assess the validity of the model, in Figure 7 we simulate the absorption spectrum of TQB using the model Hamiltonian developed. In this case, as shown inset and described in the methods section, the spectrum is obtained by a Fourier transfer of the autocorrelation function of the initial wavefunction in the ground state and the wavefunction at time, t after vertical projection into the S_1 state. The resulting spectrum compares very well with the spectrum recorded experimentally with the vibronic transitions, associated with the proton transfer (ν_1) clearly visible. Interestingly the width of the experimental spectrum is reproduced using a damping factor on the autocorrelation function of 20 fs. This is to say that after 20 fs, the excited state wavefunction does not overlap spatially with the initial ground state wavefunction. This is consistent with the proton transfer dynamics observed

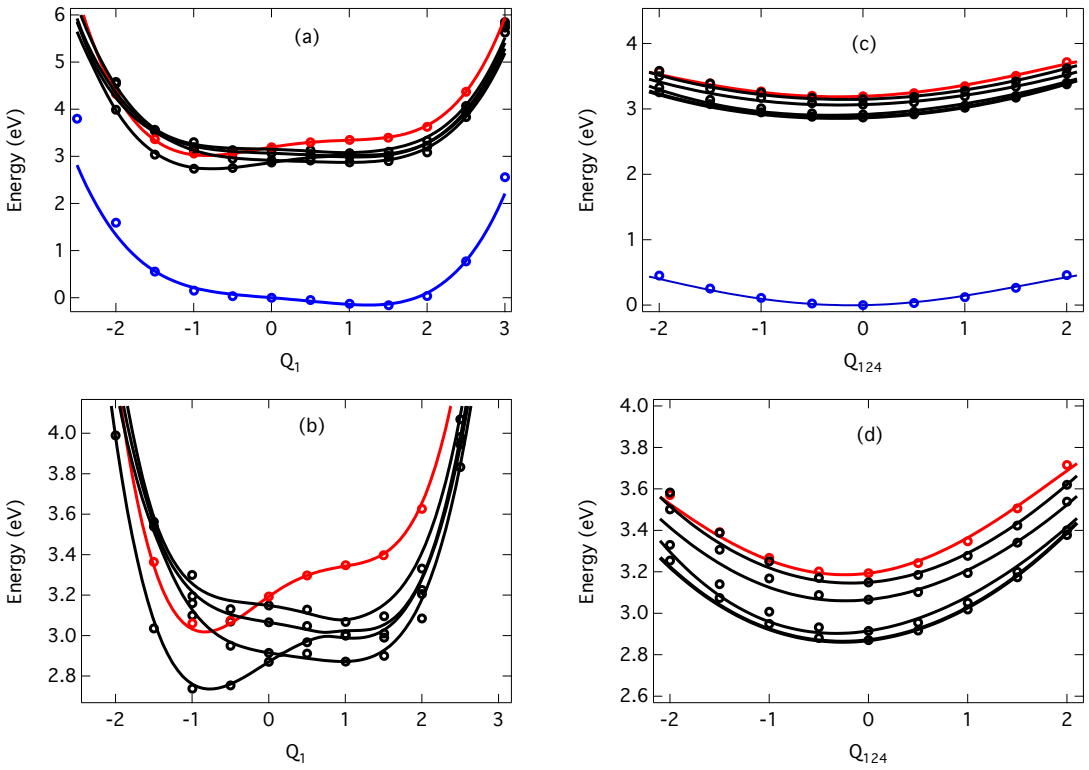

Figure 6: Cuts through the spin-free potential energy surfaces along (a) ν_1 and (c) ν_{124}. Blue is the ground state, red is the singlet excited state and black are the triplet excited states. The dots are derived from the TDDFT calculations. The lines correspond to their fit from which the expansion coefficients of the diabatic vibronic coupling Hamiltonian are determined. (b) and (d) show a zoom into the excited state surfaces.

in Figure 3 in which after the initial proton transfer the wavepacket in the S_1 state becomes localised in the S_1 minimum.

Having established the accuracy of the model, Figure 8 shows the excited state dynamics performed using this Hamiltonian. Figure 8a shows the population of the triplet states during 3.0 ps of excited state dynamics. These dynamics have been initiated from the minimum on the S_1 state, because initial relaxation of the TQB into the TQB-TB minimum on the S_1 surface has been shown to occur on a timescale (<50 fs) much faster than the rate of ISC. While the population of the triplets remains small within this timescale, a clear consistent rise is observed and corresponds to a ISC rate of 3×10^7 s^{-1}. This is in very good agreement with the rate reported experimentally[18] and consistent with the small SOCME calculated.

Figure 8b shows the fractional population of the triplet states during the same dynamics.

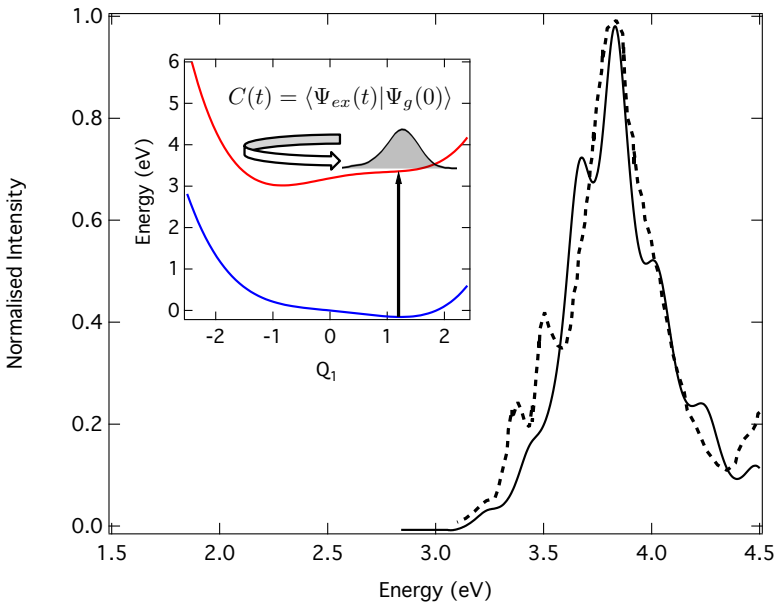

Figure 7: Experimental (dashed)[18] and theoretical (solid) absorption spectrum. The latter has been calculated using the Fourier Transform of the autocorrelation function of the initial wavefunction as described in the method section and illustrated inset.

This indicates that the diabatic T_2 state is initially populated, this is consistent with the observation that at the TQB-TB geometry this state has both the largest SOC to the S_1 state and is close to degenerate. Subsequently, the strong coupling between the triplet states means that within 500 fs an equilibrium is established and the excited state population is distributed throughout all of the triplet states. This equilibrium will persist until vibrational cooling at longer times. Importantly, because there is significant population in the higher lying excited states, (T_2, T_3 and T_4) all of which favour the TQB-TA form, a significant portion of the excited triplet states will be trapped in the TQB-TA by the barrier along the proton transfer.

In ref.,[18] the authors demonstrated that rISC in DPEPO occurs with a quantum yield of 10% and an activation energy of 0.20 eV. As shown in Table S5 this energy gap is much smaller than the S_1-T_1 energy gap at the TQB-TB structure regardless of the method used. Instead, as shown in Figure 6b, it is in good agreement with the energy gap between the S_1 state at the TQB-TB geometry and the T_1 state at the TQB-TA geometry, of 0.18 eV.

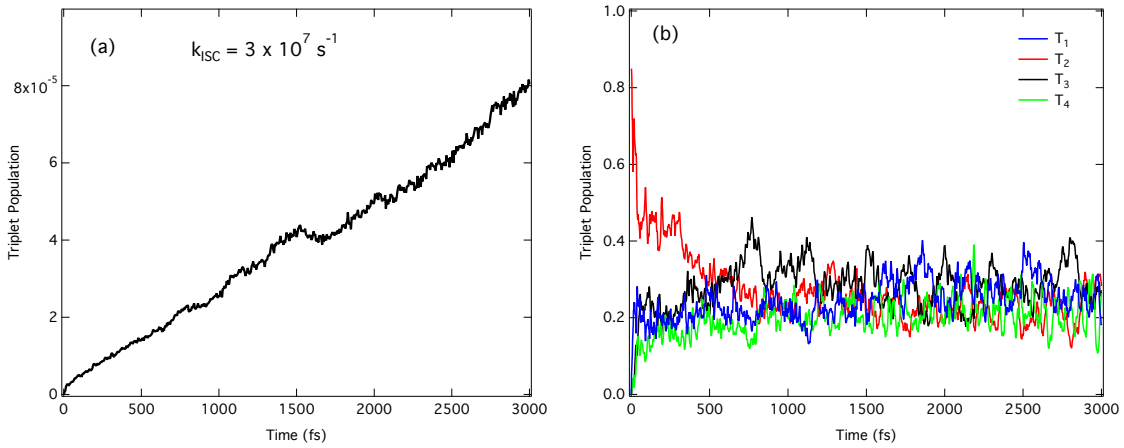

Figure 8: (a) The total fractional population of the triplet states during the first 3.0 ps after initial excitation into the minimum on the S_1 state (TQB-TB). (b) The fractional population distribution amongst the triplet states from the dynamics in(a) illustrating that although initially the T_2 is populated, the wavefunction is distributed throughout all of the triplet states within 500 fs.

Using our calculated k_{ISC}, ΔE=0.18 eV corresponding to the ^{3}TQB-TA-^{1}TQB-TB energy gap and the following relationship:

$$\frac{k_{rISC}}{k_{ISC}} = \frac{1}{3} exp(-\Delta E/k_b T) \tag{5}$$

we find a predicted k_{rISC}=7×10^3 s^{-1}, in agreement with Mamada *et al.* This is a slow triplet harvesting rate. However fast rISC is not always required for efficient TADF. Indeed, provided nonradiative rates are sufficiently suppressed,[41] rISC and TADF can still be efficient, as recently demonstrated by Noda *et al.*[42] However, high rates of rISC are preferable for reducing effects such as triplet-triplet annihilation and triplet-polaron quenching. Crucially, this mechanism would suggest that the T_1 state at the TQB-TB geometry is not harvested with TADF, as the energy gap is too large. It is stressed that while this calculated gap will be somewhat functional dependent, Table S4 shows that regardless of the method used it is typically found to be >0.35 eV, leading to k_{rISC} ∼8×10^0 s^{-1}. Smaller value of ∼0.25 eV are found with BLYP and PBE functionals, but these provide little agreement with the absolute energies and should therefore be considered cautiously.

3.4 Mechanism of Triplet Harvesting

The dynamics raises questions about mechanism for high device performance. Under electrical excitation, Mamada *et al.*[18] assumed that the triplet excitons would be most likely to form by charge carrier recombination directly in the TQB-TA form. This would enable triplet harvesting from the T_1 in TQB-TA as described in the previous section and therefore would be sufficient to describe the device performance. As shown Figure 9, the triplet energy of TQB-TA remains sufficiently low compared to that of DPEPO to provide confinement, although in this case the transport properties of DPEPO limits its device performance.[18] For CzSi and PPT, which exhibit the highest OLED EQE, the gap of ~0.1 eV is smaller than DPEPO and therefore while confinement can still be achieved, some exciton loss could be expected. For the lowest device performances, mCBP and CBP cannot confine the TQB-TA triplet excitons, but are sufficiently high to confine the TQB-TB triplet excitons.

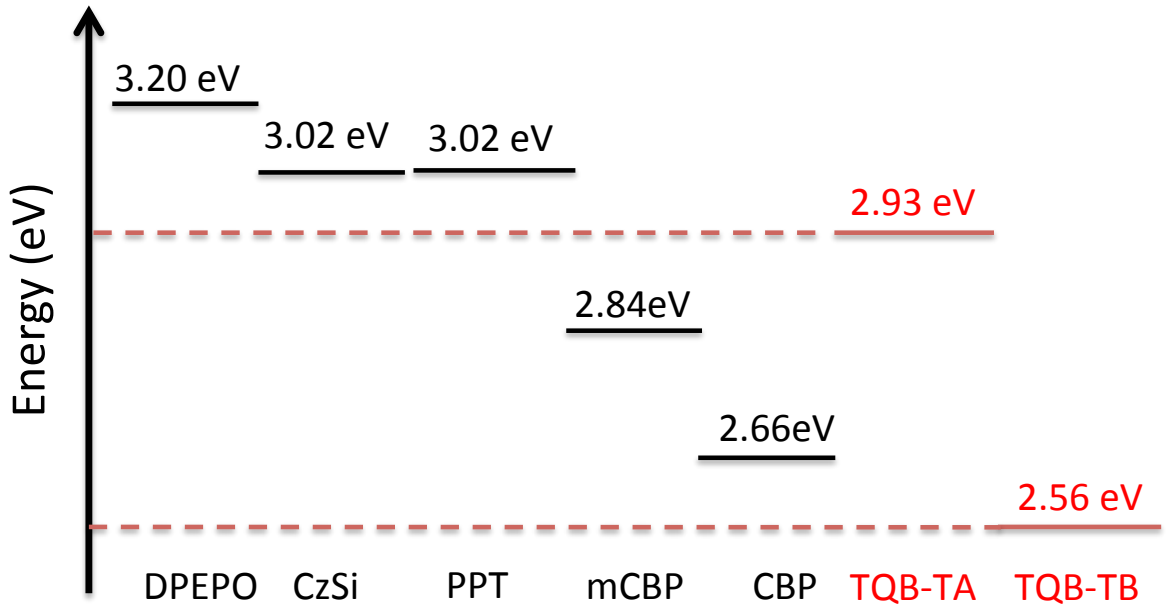

Figure 9: The T_1 energies of the 5 host materials, PPT,[50] DPEPO,[51] CzSi,[52] mCBP,[53] CBP[53] with the T_1 energy of TQB in the TQB-TA and TQB-TB forms.

A key difference in electroluminescence in contrast to photoluminescence is that the excited state is formed by the sequential trapping of charge carriers (electrons and holes).

Prior to formation of the exciton, the emitter will therefore exhibit an intermediate which either cationic or anionic form, depending on which charge arrives first. Once the first charge is trapped, structural changes can significantly affect the initial conditions of the excited state generated. Figure 10 shows the potential energy surface along ν_1 for the neutral, cationic and anionic form of TQB. While the neutral form (blue) favours TQB-TA, the lowest energy conformer for both charged forms is TQB-TB. However the relative positions of these minima compared to the neutral form means that exciton generation can be expect in both the TQB-TA and TQB-TB forms. This is consistent with previous work which demonstrated that exciton generation through injection of electron and holes exhibits the ability to form both species (enol and tautomer).[44,45]

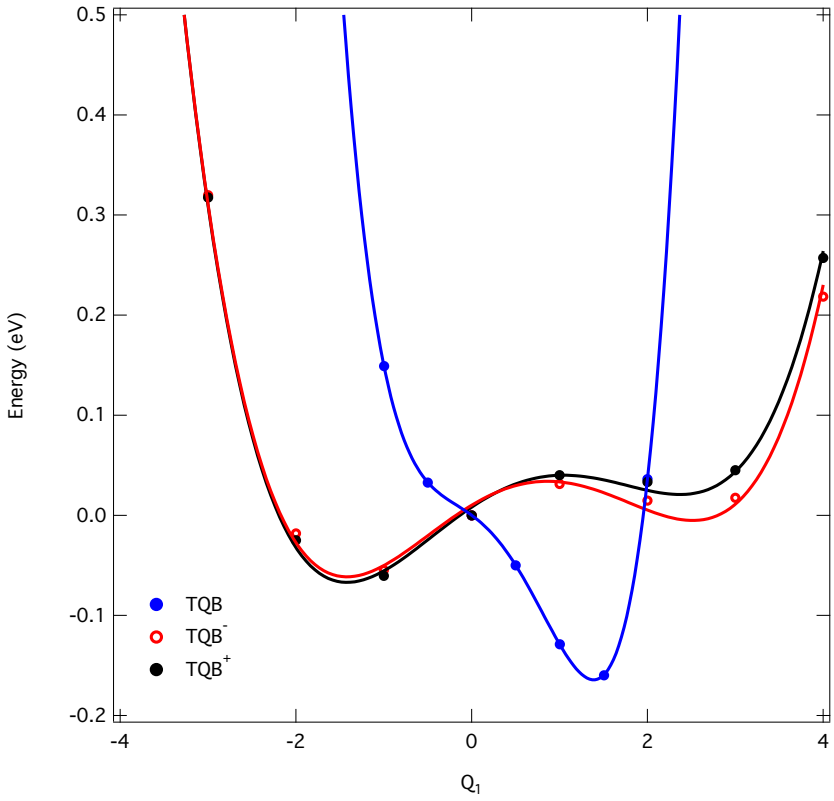

Figure 10: Ground state potential energy surface and corresponding fits along ν_1 for the neutral (blue), cationic (black) and anionic (red) states of TQB.

Finally, our present simulations suggest that TQB-TB is unfavourable due to the large energy gap between the T_1 and S_1 states. However, the device performance reported in ref.[18]

requires a >0.85 quantum yield for triplet harvesting. The delayed fluorescence lifetime upon photoexcitation, is reported to be ∼0.2 ms, much longer than those observed in efficient TADF emitters with few microsecond timeframe[46] and consistent with a calculated k_{rISC} reported above. This would appear inconsistent with the large quantum yield for triplet harvesting. However, Mordzinski *et al.*[47] have previously reported that in ESIPT molecules under high triplet-state concentrations the excited state decay is mainly governed by triplet-triplet annihilation (TTA). Although Mamada *et al.*[18] used laser power dependence to rule out TTA, this was for photoexcited samples and therefore, due to the slow rate of ISC, the concentration of triplet states is low. This is confirmed by the challenges associated with obtaining the phosphorescence spectrum.[46] TADF operating alongside TTA has previously been observed[9,54–56,59] and can provide an efficient route for higher efficiency OLED devices. Our present work cannot prove the presence of TTA, instead, experiments on the excited state dynamics under electroluminescence conditions are required. However, future theoretical work should consider the details of the initial conditions of the excited state formed by charge recombination in contrast to photoexcitation which are likely to have an important role in describing the device performance.

4 Conclusions

Diversifying molecular architectures capable of achieving TADF is crucial, not only to obtain high performance stable TADF emitters, but also for allowing a more detailed understanding into the mechanism of TADF and the differences between photo and electrical excitation important for analysis in a device context.[60] In the present work we have used quantum chemistry, molecular and quantum dynamics simulations to understand the excited state dynamics for TQB which achieves triplet harvesting by excited state intramolecular proton transfer.

Our simulations have shown that proton transfer (TQB-TA→TQB-TB) in the S_1 is ultra-

fast occurring along a barrierless excited singlet potential energy surface. This is consistent with recent experiments[46] which demonstrated that the TQB-TA could not be observed in transient absorption measurements with a temporal resolution of 5 ps. Although clearly time-resolved data with a higher time resolution is required to confirm the rate reported here. However importantly, this is not the case for the lowest triplet state, due to crossings between multiple lying excited triplet states leading to a barrier which can trap excited state population in the TQB-TA form. In contrast to most TADF emitters based upon D-A structures, the structural reorganisation in the excited state leads to an increase in the S_1 radiative rate, despite the generation of a state exhibiting CT character. This is favourable to efficient emission.

The energy gap between the singlet state of TQB-TB and the triplet of TQB-TA is $\sim$0.18 eV in agreement with the activation energy reported for TADF.[18] However at the TQB-TB geometry, a large singlet-triplet energy gap is observed, which will restrict triplet harvesting at this geometry. It is possible that direct exciton generation occurs in the TQB-TA form which would allow efficient triplet harvesting via the proposed ^{3}TQB-TA$\rightarrow{}^1$TQB-TB mechanism. Alternatively, due to the high triplet-state concentrations in the OLED, a contribution from TTA[47] arising from the lowest triplet in the TQB-TB form could occur. Both the nature of exciton generation and the initial conditions of the excited states formed and the potential for TTA requires detailed theoretical and experimental work, which will be the focus of future work.

Support Information

The Supporting Information is available free of charge on the ACS Publications website at DOI: It contains details of the Spin-vibronic Hamiltonian, additional quantum chemistry calculations on the functional dependence of the singlet-triplet gap.

Acknowledgements

We gratefully acknowledges support from the EPSRC through grants EP/N028511/1, EP/R021503/1 and EP/P012388/1.

References

(1) Endo, A.; Ogasawara, M.; Takahashi, A.; Yokoyama, D.; Kato, Y.; Adachi, C. *Thermally Activated Delayed Fluorescence from Sn4+-Porphyrin Complexes and Their Application to Organic Light Emitting Diodes - A Novel Mechanism for Electroluminescence Adv. Mater.* **2009**, *21*, 4802–4806.

(2) Uoyama, H.; Goushi, K.; Shizu, K.; Nomura, H.; Adachi, C. *Highly Efficient Organic Light-Emitting Diodes From Delayed Fluorescence Nature* **2012**, *492*, 234–238.

(3) Nakanotani, H.; Furukawa, T.; Hosokai, T.; Hatakeyama, T.; Adachi, C. *Light Amplification in Molecules Exhibiting Thermally Activated Delayed Fluorescence Adv. Opt. Mater.* **2017**, *5*, 1700051.

(4) Kuehne, A. J.; Gather, M. C. *Organic Lasers: Recent Developments on Materials, Device Geometries, and Fabrication Techniques Chem. Rev.* **2016**, *116*, 12823–12864.

(5) Chang, W.; Congreve, D. N.; Hontz, E.; Bahlke, M. E.; McMahon, D. P.; Reineke, S.; Wu, T. C.; Bulović, V.; Van Voorhis, T.; Baldo, M. A. *Spin-Dependent Charge Transfer State Design Rules in Organic Photovoltaics Nat. Comm.* **2015**, *6*, 6415.

(6) Freeman, D. M.; Musser, A. J.; Frost, J. M.; Stern, H. L.; Forster, A. K.; Fallon, K. J.; Rapidis, A. G.; Cacialli, F.; McCulloch, I.; Clarke, T. M. et al. *Synthesis and Exciton Dynamics of Donor-Orthogonal Acceptor Conjugated Polymers: Reducing the Singlet–Triplet Energy Gap J. Am. Chem. Soc.* **2017**, *139*, 11073–11080.

(7) Wong, M. Y.; Zysman-Colman, E. *Purely Organic Thermally Activated Delayed Fluorescence Materials for Organic Light-Emitting Diodes Adv. Mater.* **2017**, *29*, 1605444

(8) Penfold, T.; Dias, F.; Monkman, A. *The Theory of Thermally Activated Delayed Fluorescence for Organic Light Emitting Diodes Chem. Comm.* **2018**, *54*, 3926–3935.

(9) Dias, F. B.; Bourdakos, K. N.; Jankus, V.; Moss, K. C.; Kamtekar, K. T.; Bhalla, V.; Santos, J.; Bryce, M. R.; Monkman, A. P. *Triplet Harvesting with 100% Efficiency by Way of Thermally Activated Delayed Fluorescence in Charge Transfer OLED Emitters Adv. Mater.* **2013**, *25*, 3707–3714.

(10) Penfold, T. J. *On Predicting the Excited-State Properties of Thermally Activated Delayed Fluorescence Emitters J. Phys. Chem. C* **2015**, *119*,13535–13544 .

(11) Yersin, H. *Triplet Emitters for OLED Applications. Mechanisms of Exciton Trapping and Control of Emission Properties Transition Metal and Rare Earth Compounds*; Springer, 2004; 1–26.

(12) Hatakeyama, T.; Shiren, K.; Nakajima, K.; Nomura, S.; Nakatsuka, S.; Kinoshita, K.; Ni, J.; Ono, Y.; Ikuta, T. *Ultrapure Blue Thermally Activated Delayed Fluorescence Molecules: Efficient HOMO–LUMO Separation by the Multiple Resonance Effect Adv. Mater.* **2016**, *28*, 2777–2781.

(13) Northey, T.; Penfold, T. *The Intersystem Crossing Mechanism of an Ultrapure Blue Organoboron Emitter Org. Elec.* **2018**, *12*, 1988–1991.

(14) Penfold, T.; Gindensperger, E.; Daniel, C.; Marian, C. *Spin-vibronic Mechanism for Intersystem Crossing Chem. Rev.* **2018**, *118*, 6975–7025

(15) Gibson, J.; Monkman, A.; Penfold, T. *The Importance of Vibronic Coupling for Efficient Reverse Intersystem Crossing in TADF Molecules ChemPhysChem* **2016**, *17*, 2956-2961.

(16) Etherington, M. K.; Gibson, J.; Higginbotham, H. F.; Penfold, T. J.; Monkman, A. P. *Revealing the Spin–Vibronic Coupling Mechanism of Thermally Activated Delayed Fluorescence Nat. Comm.* **2016**, *7*, 13680.

(17) Gibson, J.; Penfold, T. *Nonadiabatic Coupling Reduces the Activation Energy in Thermally Activated Delayed Fluorescence Phys. Chem. Chem. Phys.* **2017**, *19*, 8428–8434.

(18) Mamada, M.; Inada, K.; Komino, T.; Potscavage Jr, W. J.; Nakanotani, H.; Adachi, C. *Highly Efficient Thermally Activated Delayed Fluorescence from an Excited-State Intramolecular Proton Transfer System ACS Cent. Sci.* **2017**, *3*, 769–777.

(19) Zhao, J.; Ji, S.; Chen, Y.; Guo, H.; Yang, P. *Excited State Intramolecular Proton Transfer (ESIPT): From Principal Photophysics to the Development of New Chromophores and Applications in Fluorescent Molecular Probes and Luminescent Materials Phys. Chem. Chem. Phys.* **2012**, *14*, 8803–8817.

(20) Seo, J.; Kim, S.; Park, S. Y. *Strong Solvatochromic Fluorescence From the Intramolecular Charge-Transfer State Created by Excited-State Intramolecular Proton Transfer J. Am. Chem. Soc.* **2004**, *126*, 11154–11155.

(21) Kwon, J. E.; Park, S. Y. *Advanced Organic Optoelectronic Materials: Harnessing Excited-State Intramolecular Proton Transfer (ESIPT) Process Adv. Mater.* **2011**, *23*, 3615–3642.

(22) Park, S.; Kwon, O.-H.; Lee, Y.-S.; Jang, D.-J.; Park, S. Y. *Imidazole-Based Excited-State Intramolecular Proton-Transfer (ESIPT) Materials: Observation of Thermally Activated Delayed Fluorescence (TDF) J. Phys. Chem. A* **2007**, *111*, 9649–9653.

(23) Padalkar, V. S.; Seki, S. *Excited-State Intramolecular Proton-Transfer (ESIPT)-Inspired Solid State Emitters Chem. Soc. Rev.* **2016**, *45*, 169–202.

(24) Hirata, S.; Head-Gordon, M. *Time-Dependent Density Functional Theory within the Tamm-Dancoff Approximation Chem. Phys. Lett.* **1999**, *314*, 291–299.

(25) Perdew, J. P.; Burke, K.; Ernzerhof, M. *Generalized Gradient Approximation Made Simple Phys. Rev. Lett.* **1996**, *77*, 3865–3868.

(26) Adamo, C.; Barone, V. *Toward Reliable Density Functional Methods Without Adjustable Parameters: The PBE0 Model J. Chem. Phys.* **1999**, *110*, 6158–6170.

(27) Shao, Y; Gan, Z.; Epifanovsky, E.; Gilbert, A.T.B.; Wormit, M.; Kussmann, J.; Lange, A. W.; Behn, A.; Deng, J.; Feng, X.; et al. *Advances in Molecular Quantum Chemistry Contained in the Q-Chem 4 Program Package Mol. Phys.* **2015**, *113*, 184–215.

(28) Weigend, F. *Accurate Coulomb-Fitting Basis Sets for H to Rn Phys. Chem. Chem. Phys.* **2006**, *8*, 1057–1065.

(29) Tomasi, J.; Mennucci, B.; Cammi, R. *Quantum Mechanical Continuum Solvation Models Chem. Rev.* **2005**, *105*, 2999–3094.

(30) Cammi, R.; Corni, S.; Mennucci, B.; Tomasi, J. *Electronic Excitation Energies of Molecules in Solution: State Specific and Linear Response Methods for Nonequilibrium Continuum Solvation Models J. Chem. Phys.* **2005**, *122*, 104513.

(31) Ufimtsev, I. S.; Martínez, T. J. *Quantum Chemistry on Graphical Processing Units. 1. Strategies for Two-Electron Integral Evaluation J. Chem. Theory Comput.* **2008**, *4*, 222–231.

(32) Ufimtsev, I. S.; Martínez, T. J. *Quantum Chemistry on Graphical Processing Units. 3. Analytical Energy Gradients, Geometry Optimization, and First Principles Molecular Dynamics J. Chem. Theory Comput.* **2009**, *5*, 2619–2628.

(33) Capano, G.; Chergui, M.; Rothlisberger, U.; Tavernelli, I.; Penfold, T. J. *A Quantum*

Dynamics Study of the Ultrafast Relaxation in a Prototypical Cu(I)–Phenanthroline J. Phys. Chem. A **2014**, *118*, 9861–9869..

(34) Eng, J.; Gourlaouen, C.; Gindensperger, E.; Daniel, C. *Spin-Vibronic Quantum Dynamics for Ultrafast Excited-State Processes Acc. Chem. Res.* **2015**, *48*, 809–817.

(35) Meyer, H.-D., Gatti, F., Worth, G. A., Eds. *High Dimensional Quantum Dynamics: Basic Theory, Extensions, and Applications of the MCTDH method*; VCH: Weinheim, Germany, 2008.

(36) Köppel, H.; Domcke, W.; Cederbaum, L. S. *Multimode Molecular Dynamics Beyond the Born-Oppenheimer Approximation Adv. Chem. Phys.* **1984**, *57*, 59–246.

(37) Penfold, T.; Spesyvtsev, R.; Kirkby, O. M.; Minns, R.; Parker, D.; Fielding, H.; Worth, G. *Quantum Dynamics Study of the Competing Ultrafast Intersystem Crossing and Internal Conversion in the "Channel 3" Region of Benzene J. Chem. Phys.* **2012**, *137*, 204310.

(38) Meyer, H.-D.; Manthe, U.; Cederbaum, L. S. *The Multi-Configurational Time-Dependent Hartree Approach Chem. Phys. Lett.* **1990**, *165*, 73–78.

(39) Beck, M. H.; Jäckle, A.; Worth, G. A.; Meyer, H.-D. *The Multiconfiguration Time-Dependent Hartree Method: A Highly Efficient Algorithm for Propagating Wavepackets. Phys. Rep.* **2000**, *324*, 1–105.

(40) Northey, T.; Stacey, J.; Penfold, T. *The Role of Solid State Solvation on the Charge Transfer State of a Thermally Activated Delayed Fluorescence Emitter J. Mater. Chem. C* **2017**, *5*, 11001–11009.

(41) Turro, N. J.; Ramamurthy, V.; Scaiano, J. C. *Modern Molecular Photochemistry of Organic Molecules Photochem. Photobiol.* **2012**, *88*, 1033–1033.

(42) Noda, H..; Nakanotani, H.; Adachi, C. *Highly Efficient Thermally Activated Delayed Fluorescence with Slow Reverse Intersystem Crossing Chem. Lett.* **2018**, https://doi.org/10.1246/cl.180813 (accessed Mar 6, 2019).

(43) It is noted that depending on the energetics of the frontier orbitals of the host and guest involved, this may not necessarily always be the case. However, a more detailed analysis is beyond the scope of the present work.

(44) Tang, K C; Chang, M J; Lin, T Y; Pan, H A; Fang, T C; Chen, K Y; Hung, W Y; Hsu, Y H; Chou, P T *Fine Tuning the Energetics of Excited-State Intramolecular Proton Transfer (ESIPT): White Light Generation in a Single ESIPT System J. Am. Chem. Soc.* **2011**, *133*, 17738–17745 .

(45) Tarkka, R. M and Zhang, X; Jenekhe, S. A *Electrically Generated Intramolecular Proton Transfer: Electroluminescence and Stimulated Emission from Polymers J. Am. Chem. Soc.* **1996**, *118*, 9438–9439 .

(46) Dos-Santos, P *The Study of Thermally Activated Delayed Fluorescence Mechanism in Mono and Bimolecular Systems, Durham University Thesis.* **2018** .

(47) Mordzinski, A.; Grellmann, K. *Excited-State Proton-Transfer Reactions in 2-(2'-hydroxyphenyl) benzoxazole. Role of Triplet States J. Phys. Chem.* **1986**, *90*, 5503–5506.

(48) Kumpulainen, T.; Rosspeintner, A.; Dereka, B.; Vauthey, E. *Influence of Solvent Relaxation on Ultrafast Excited-State Proton Transfer to Solvent J. Phys. Chem. Lett.* **2017**, *8*, 4516–4521.

(49) Adachi, C.; Baldo, M. A.; Forrest, S. R. *Electroluminescence Mechanisms in Organic Light Emitting Devices Employing a Europium Chelate Doped in a Wide Energy Gap Bipolar Conducting Host J. Appl. Phys.* **2000**, *87*, 8049–8055.

(50) Kang, J. S.; Hong, T. R.; Kim, H. J; Son, Y. H.; Lampande, R.; Kang, B. Y. ; Lee, C.; Bin, J K.; Lee, B. S.; Yang, J. H.; et al. *High-Performance Bipolar Host Materials for Blue TADF Devices with Excellent External Quantum Efficiencies J. Mater. Chem. C* **2016**, *4*, 4512–4520.

(51) Zhang, Q.; Li, B.; Huang, S.; Nomura, H.; Tanaka, H.; Adachi, C. *Efficient Blue Organic Light-Emitting Diodes Employing Thermally Activated Delayed Fluorescence Nat. Photonics* **2014**, *8*, 326–332.

(52) Tsai, M.-H.; Lin, H.-W.; Su, H.-C.; Ke, T.-H.; Wu, C.-C.; Fang, F.-C.; Liao, Y.-L.; Wong, K.-T.; Wu, C.-I. *Highly Efficient Organic Blue Electrophosphorescent Devices Based on 3, 6-bis (triphenylsilyl) Carbazole as the Host Material Adv. Mater.* **2006**, *18*, 1216–1220.

(53) Gong, S.; He, X.; Chen, Y.; Jiang, Z.; Zhong, C.; Ma, D.; Qin, J.; Yang, C. *Simple CBP Isomers with High Triplet Energies for Highly Efficient Blue Electrophosphorescence J. Mater. Chem.* **2012**, *22*, 2894–2899.

(54) Jankus, V.; Chiang, C.-J.; Dias, F.; Monkman, A. P. *Deep Blue Exciplex Organic Light-Emitting Diodes with Enhanced Efficiency; P-type or E-type Triplet Conversion to Singlet Excitons? Adv. Mater.* **2013**, *25*, 1455–1459.

(55) Ward, J. S.; Nobuyasu, R. S.; Batsanov, A. S.; Data, P.; Monkman, A. P.; Dias, F. B.; Bryce, M. R. *The Interplay of Thermally Activated Delayed Fluorescence (TADF) and Room Temperature Organic Phosphorescence in Sterically-Constrained Donor–Acceptor Charge-Transfer Molecules Chem. Commun.* **2016**, *52*, 2612–2615

(56) Huang, R.; Ward, J. S.; Kukhta, N. A.; Avó, J.; Gibson, J.; Penfold, T. J.; Lima, J. C.; Batsanov, A. S.; Berberan-Santos, M. N.; Bryce, M. R.; et al. *The Influence of Molecular Conformation on the Photophysics of Organic Room Temperature Phosphorescent Luminophores J. Mater. Chem. C* **2018**, *6*, 9238–9247.

(57) Dias, F. B.; Penfold, T. J.; Monkman, A. P. *Photophysics of Thermally Activated Delayed Fluorescence Molecules Methods Appl. Fluoresc.* **2017**, *5*, 012001.

(58) Ganzorig, C.; Fujihira, M. *A Possible Mechanism for Enhanced Electrofluorescence Emission Through Triplet–Triplet Annihilation in Organic Electroluminescent Devices App. Phys. Lett.* **2002**, *81*, 3137–3139.

(59) Chen, P.; Wang, L P.; Tan, W Y.; Peng, Q M.; Zhang, ST.; Zhu, X H.; Li, F. *Delayed Fluorescence in a Solution-Processable Pure Red Molecular Organic Emitter Based on Dithienylbenzothiadiazole: A Joint Optical, Electroluminescence, and Magnetoelectroluminescence Study ACS Appl. Mater. Interfaces* **2015**, *7*, 2972–2978.

(60) Palmeira, T.; Berberan-Santos, M. N. *Kinetic Criteria for Optimal Thermally Activated Delayed Fluorescence in Photoluminescence and in Electroluminescence J. Phys. Chem. C* **2016**, *121*, 701–708

.

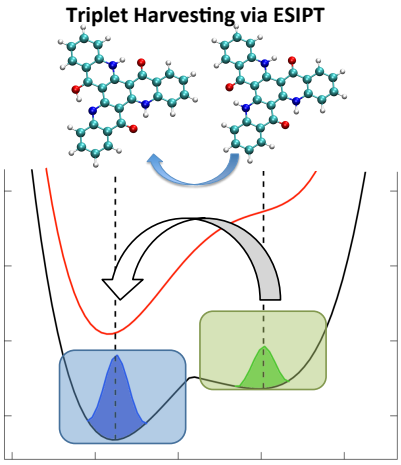
Triplet Harvesting via ESIPT

Thomas Penfold was awarded his Ph.D. in 2010 from the University of Birmingham, United Kingdom, under the guidance of Prof. Graham Worth. He subsequently joined the group of Prof. Majed Chergui at the cole Polytechnique Fdrale de Lausanne, Switzerland before spending two years within the SwissFEL project at the Paul Scherrer Institut, Switzerland. He joined Newcastle University in 2015 as Lecturer in Theoretical and Computational Chemistry. His current research interests include quantum dynamics, time-resolved spectroscopy, and excited state dynamics of organic and inorganic systems. His group has recently worked extensively upon providing new insights into the mechanism for thermally activated delayed fluorescence. The overall objective of his research is to provide develop fundamental understanding into design rules for molecules and materials which operate in electronically excited states.